Integrative Biology

Accepted Manuscript

This article can be cited before page numbers have been issued, to do this please use: A. Fanti, L. Gammuto, F. Mavelli, P. Stano and R. Marangoni, *Integr. Biol.*, 2017, DOI: 10.1039/C7IB00138J.

ROYAL SOCIETY OF CHEMISTRY

rsc.li/integrative-biology

View Article Online
DOI: 10.1039/C7IB00138J

By combining experimental and modelling, this study provides a first evidence of macromolecular preferential retention (over small molecules) inside POPC vesicles during vesicle fragmentation (division) by mechanical extrusion. The true heterogeneous nature of vesicles originated by spontaneous self-assembly ("vesicle diversity") is also highlighted.
Its relevance is twofold. First, when lipid vesicles are intended as primitive cell models, this result suggest how and why macromolecules are entrapped, stored, and transmitted over protocell division, allowing the emergence of living cells. Second, this work contributes to the ongoing research on lipid vesicles used as synthetic cell-like structures in bottom-up synthetic biology, by a detailed characterization of giant vesicle extrusion (which can be a viable route to prepare solute-filled conventional vesicles otherwise difficult to obtain).

View Article Online
DOI: 10.1039/C7IB00138J
ROYAL SOCIETY OF CHEMISTRY

Journal Name

ARTICLE TYPE

Cite this: DOI: 10.1039/xxxxxxxxxx

Do protocells preferentially retain macromolecular solutes upon division/fragmentation? A study based on the extrusion of POPC giant vesicles.

Alessio Fanti,[†a] Leandro Gammuto,[†a] Fabio Mavelli,[b] Pasquale Stano,[‡c*] and Roberto Marangoni[a,d*]

Received Date
Accepted Date

DOI: 10.1039/xxxxxxxxxx

www.rsc.org/journalname

A key process of protocell behaviour is their recursive growth and division. In order to be sustainable, the latter must be characterized by an even and homogeneous partition of the solute molecules initially present in the parent protocell among the daughter ones. Here we have investigate, by means of an artificial division model (extrusion of giant lipid vesicles) and confocal microscopy, the fate of solutes when a large vesicle fragments into many smaller vesicles. Solutes of low- and high-molecular weight such as pyranine, calcein, albumin-FITC, dextran-FITC and carbonic anhydrase have been employed. Although the vesicle extrusion brings about a release of their inner content in the environment, the results shown in this initial report indicate that macromolecules can be partially retained when compared with low-molecular weight ones. Results are discussed from the viewpoint of the life cycle of primitive cells. In particular, the findings suggest that a similar mechanism operating during the critical step of vesicle growth-division could have contributed to primitive evolution.

1 Introduction

One of the major goals of synthetic biology is the creation of synthetic minimal cell models for addressing open questions in the biology domain and for developing new tools for biotechnology [1–3]. Ongoing research on primitive cells models and artificial prototype cells (here both indicated as 'protocells') benefits from a synthetic biology approach. It adopts the constructive paradigm (understanding by building) and integrates quantitative analysis with mathematical tools. Lipid vesicles (liposomes) are often used to build cellular models of various complexity. These models range from 'empty' fatty acid vesicles, for instance those that are able undergoing spontaneous self-reproduction [4–6], up to much more complex systems, such as those hosting in the vesicle lumen the whole transcription-translation biomachinery [7–11].

When protocells are studied for deciphering some physical aspect of primitive cells formation and proliferation, the capture and the retention of molecular solutes are two fundamental features to consider. With respect to solute capture, it has been shown that when vesicles formation occurs in a protein- or nucleic acid- solution, vesicles easily entrap these solutes in their lumen [12–14]. Recent observations have revealed that under certain conditions, a small number of vesicles results filled with a very high number of solute molecules [15–18].

With respect to the second issue (solute retention), the starting, and perhaps obvious, consideration is that in order to proliferate, protocells have to grow and divide. The self-reproduction of fatty acid vesicles have been reported [4–6], but with few exceptions [5,19–22] not much interest has been devoted to understand what happens to the encapsulated molecules during growth/division. Starting from a functional 'mother' protocell, similarly functional 'daughter' protocells can be obtained only if the molecules initially contained in the mother are evenly redistributed among the daughters. Protocell proliferation can be seriously hampered by solute loss or unpaired solute redistribution. In other words, while solute capture is a fundamental step for protocell emergence from separated components, protocells self-reproduction (growth/division) must be especially robust with respect to the retention and partition of the entrapped molecules [23].

Here we present an experimental and computational study on vesicle formation and solute capture, followed by vesicle fragmentation and solute partition. The study has been carried out to mimic the formation of protocells from another protocell, following a process of growth-division. Our experimental model is

[a] *Biology Department, University of Pisa; Via Derna 1, I-56126 Pisa, Italy. Tel: (+39) 050 2211525; Fax: (+39) 050 2211527; e-mail: roberto.marangoni@unipi.it*
[b] *Chemistry Department, University of Bari; Via E. Orabona 4, I-70125, Bari, Italy.*
[c] *Science Department, Roma Tre University; Viale G. Marconi 446, I-00146 Rome, Italy.*
[d] *CNR – Institute of Biophysics; Via G. Moruzzi 1, I-56124 Pisa, Italy.*
† These authors contributed equally to this work
‡ Current address: *DiSTeBA, University of Salento; Ecotekne, I-73100 Lecce, Italy. Tel. (+39) 0832 298709; Fax: (+39) 0832 298732 e-mail: pasquale.stano@unisalento.it*
∗ Joint Corresponding-Authors

View Article Online
DOI: 10.1039/C7IB00138J

based on (*i*) the spontaneous formation of solute-filled phospholipid giant vesicles (GVs) (Fig.1a), and (*ii*) their fragmentation in several small daughter vesicles via a mechanical process[24] that simulates protocell self-reproduction[21] (Fig.1b). In other words, we have simply applied the extrusion method as a way to create many small daughter vesicles from large ones (the mothers). Although it has been suggested that such an approach could model protocell division in porous rocks[21], it should be recalled that operating under conditions favouring spontaneous vesicle division, i.e., by addition or production of membrane-forming compounds[6,25–27], would be a better model for addressing the solute retention problem.

Based on the experimentally obtained GVs populations, we constructed *in silico* vesicles undergoing the same transformations than real vesicles (Fig.1c). *In silico* vesicle populations strictly obey to physico-chemical rules and follow purely random stochastic paths. The *in silico* vesicles can be useful for hypothesis testing, just by contrasting their behaviour with the experimental outcomes. By combining wet-lab experiments and numerical modelling, here we provide novel evidences on the retention and partition of solutes, in particular with respect to their molecular weight (MW). Larger molecules are retained much better than small molecules. This might suggest that a basic physical mechanisms (based on solute size) could have been a source of selective pressure in prebiotic times, favouring the transition from small to large molecules, as the latter one are better retained during vesicle division. Such a mechanism could operate before the onset of sophisticated control mechanism of solute partition during the key event of cell reproduction.

2 Results

We have applied a combination of bottom-up synthetic biology and systems biology, blending experimental approaches and theoretical modelling (Fig. 1). The experimental model is based on the preparation of giant lipid vesicles (GVs) by the natural swelling method (Fig. 1a), followed by a mechanical GVs division to give conventional sub-micron vesicles by the extrusion technique (VETs) (Fig. 1b). GVs contained solutes with different MW (from 0.5 to 150 kDa) and different chemical structures. We have measured size and content of vesicles before and after extrusion and compared with the null hypotheses:

- before extrusion: $H_{0,\mathrm{I}}$, the mean intra-GVs solute concentration, $\langle C_{\mathrm{GVs}} \rangle$, is equal to the bulk concentration, C_{bulk}, of the solute in the solution, which has been used to prepare the GVs; i.e., $\langle C_{\mathrm{GVs}} \rangle = C_{\mathrm{bulk}}$;
- after extrusion: $H_{0,\mathrm{II}}$, the mean intra-VETs and the mean intra-GVs solute concentrations are equal; i.e. $\langle C_{\mathrm{VETs}} \rangle = \langle C_{\mathrm{GVs}} \rangle$.

In addition to $H_{0,\mathrm{I}}$ and $H_{0,\mathrm{II}}$, we have also checked additional less-restrictive hypotheses ($h_{0,\mathrm{I}}$ and $h_{0,\mathrm{II}}$) based on the likelihood that a certain concentration value belongs or not – in a statistical sense – to a certain 'parent' distribution (see Section 5.4 for details). No statistical tests were carried out to compare the GVs *size* distributions, because they derive from a fractionation procedure

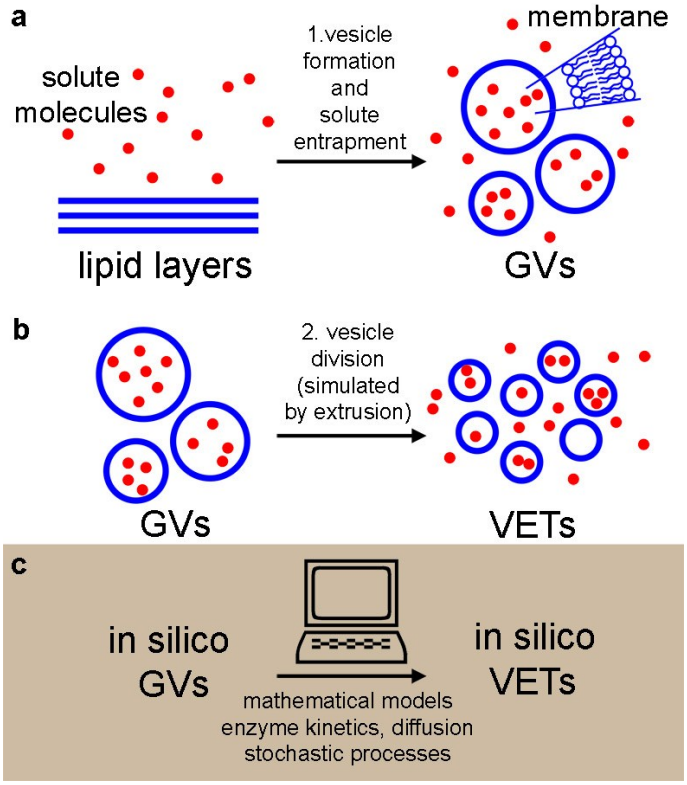

Fig. 1 Experimental and numerical approaches. (a) Giant vesicles (GVs) are formed by the natural swelling of stratified lipid layers in the presence of a solute of interest. Part of the solutes will be encapsulated, other will be free. (b) After free-solute removal, GVs are extruded in order to simulate vesicle division. Vesicles obtained by the extrusion technique (VETs) are produced. Solutes initially present inside 'mother' GVs will be partitioned among 'daughters' VETs, while some solutes will be lost in the environment. (c) Based on experimentally determined GVs parameters (size distribution, mean solute content) an *in silico* GVs population has been simulated by computational methods, then transformed in smaller vesicles. The solutes initially included in each large GV have been stochastically redistributed among the smaller VETs. *In silico* GVs and VETs have the same size distribution of the experimental samples.

View Article Online
DOI: 10.1039/C7IB00138J

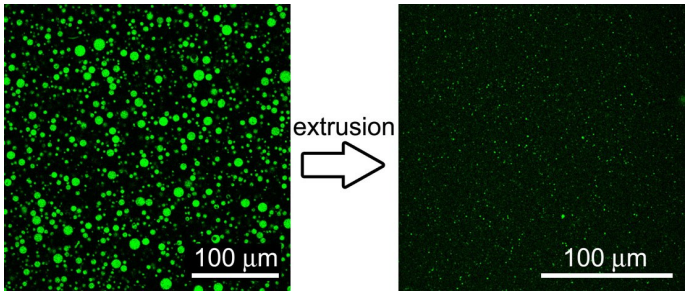

Fig. 2 Confocal fluorescence images of calcein-filled GVs (left) and VETs (right). GVs have been purified by centrifugation and extruded through polycarbonate membrane with pores diameter of 800 nm. Similar images have been recorded for the other solutes.

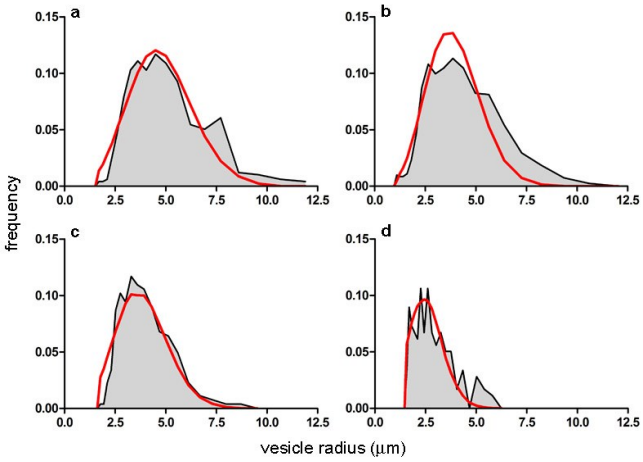

Fig. 3 Comparison between GVs size distribution as obtained experimentally (grey area) and by numerical modelling (Helfrich distribution, red curve). Size distributions refer to GVs filled with (a) pyranine; (b) calcein; (c) BSA-FITC; (d) dextran-FITC. Populations statistics are reported in Table 1.

which likely introduces both a size bias and a variance contribution that cannot be easily estimated.

In parallel to experiments, all physical processes have been simulated by stochastic numerical modelling (Fig. 1c) in order to compare the observed and the simulated patterns. Stochastic analysis is essential in vesicle population analysis, as vesicles always display heterogeneity with respect to size and content[18,28–33]. A population of solute-filled GVs has been artificially generated *in silico* and filled with solutes, based on parameters obtained by experiments. Next, the transformation of GVs in VETs is simulated by taking into account the initial and final size distributions, while the solutes have been partitioned by algorithms that model physical stochastic effects as purely random ones.

2.1 Experimental model

POPC GVs have been produced by the natural swelling method, which consists in the unperturbed swelling of a lipid film in the presence of solutes of interest. Although POPC cannot be considered a primitive lipids for the construction of protocells, it has been often used in studies when the focus is not on the chemical nature of the bilayer, rather on the solute compartmentation.[19,20,34,35] Pyranine (0.52 kDa) and calcein (0.62 kDa) have been used as low molecular weight solutes, whereas bovine serum albumin-FITC (BSA-FITC, 69 kDa), dextran-FITC (150 kDa), and carbonic anhydrase (CA, 30 kDa) as macromolecular ones. Pyranine, calcein, BSA-FITC, and dextran-FITC are fluorescent molecules, whose concentration can be easily measured. CA has been quantified by probing its esterase activity[36,37], with the fluorogenic substrate 6-carboxyfluorescein diacetate (CFDA) as discussed separately in Section 2.3.

2.1.1 GVs formation by natural swelling

Natural swelling produces GVs with a broad size distribution (up to ca. 50 μm) that is not convenient for the purpose of this study. Therefore, we firstly devise a method for isolating small GVs and with a narrower size distribution. At this aim, we adopted a centrifugation strategy that allows the fractionation of vesicles according to their size. This pre-treatment also removes non-entrapped solutes, so that GVs appear fluorescent over a dark background (Fig. 2, left).

Solute-filled GVs have been easily prepared irrespective of the type and concentration of the solute (pyranine, calcein, albumine-FITC, dextran-FITC, carbonic anhydrase). After fractionation, GVs with average radius ranging between 2.6 and 4.4 μm are obtained (Table 1), with a positively skewed size distribution (Fig.3).

According to $H_{0,I}$ (a purely stochastic entrapment scenario), when GVs form by natural swelling the expectation is that the concentration of the solutes initially present in the solution is also found inside the vesicles. This scenario purposely neglects, at least on average, the potential attractive/repulsive solute-solute and solute-lipid interactions which may play a role in the entrapment process. It simply corresponds to a random sampling, with the number of entrapped molecules only determined by the vesicle volume. We expect that, due to the very large size of GVs, intra-GVs solute concentration is equal (or very near) to the bulk solute concentration.

The internal fluorescence of individual GVs was measured by image analysis, and a distribution of concentration was obtained for each population thanks to calibration curves. Figure 4 (top line) shows the concentration-vs-radius dot-plots referring to the four GVs populations, one for each fluorescent solute. Most of the GVs containing pyranine, calcein, and BSA-FITC have internal solute concentration near the expected bulk values of, respectively, 5, 10 and 10 μM (indicated by the dashed blue lines in Fig. 4). The average intra-GVs concentrations of these solutes are, respectively, 5.4 $\pm$ 0.7 μM, 8.9 $\pm$ 1.3 μM, and 8.5 $\pm$ 2.1 μM. Contrarily, the average intra-vesicle dextran-FITC concentration is 0.79 $\pm$ 0.17 μM, quite less than the expected (1.75 μM). This might be due to considerable high molecular weight of dextran (150 kDa) which could lead to solute exclusion during lipid swelling and vesicle closure.

GVs data in Fig. 4 (top line) also point to two other facts. First, the solute concentration distribution is quite broad. This is a noteworthy fact, not consistent with random fluctuations around an average value. Fluctuations are proportional to $\sqrt{n}$, where n is

View Article Online
DOI: 10.1039/C7IB00138J

Table 1 Average vesicle radius (μm), mean $\pm$ s.d., as obtained experimentally. The number of measured vesicles is indicated in parenthesis. Note that CA-containing VETs have been obtained by extrusion through 1 μm (radius) pores, whereas the other cases refer to extrusion through 0.4 μm (radius) pores.

Solutes	GVs	VETs
pyranine	4.4 $\pm$ 1.6 (496)	0.41 $\pm$ 0.07 (4394)
calcein	3.7 $\pm$ 1.5 (814)	0.42 $\pm$ 0.13 (7554)
BSA-FITC	3.6 $\pm$ 1.1 (265)	0.46 $\pm$ 0.13 (4440)
dextran-FITC	2.6 $\pm$ 0.9 (179)	0.41 $\pm$ 0.07 (9634)
CA	3.2 $\pm$ 1.8 (285)	0.76 $\pm$ 0.34 (233)

the expected average number of entrapped solutes, that scales with the vesicle volume. In our conditions n is typically very large ($10^5 - 10^6$), so that the relative variability $\sqrt{n}/n$ should be below 1%. A much larger variation among intra-GVs solute concentration is observed, suggesting more complex (and heterogeneous) mechanisms of GVs formation and solute capture. Second, there is a weak dependence of inner solute concentration from the GVs size (this is particular evident in the case of small GVs). Again, this can be due to coexisting different mechanisms of vesicle formation (larger and smaller GVs originating in different ways). As the deeper investigation about these patterns lies outside the scope of the present paper, we postpone it to future work.

2.1.2 GVs extrusion to produce VETs

GVs were extruded by repeated passages through a polycarbonate membrane with 0.4 μm pores radius, in order to simulate in artificial way the process of vesicle division[38]. The resulting vesicles, called VETs (Fig. 2, left), have a narrow size distributions, centred as expected around a radius of 0.4 μm. Their mean sizes and the size distributions are reported in Table 1 and Fig. 5. The average VET radius of 0.41-0.42 μm is slightly larger than the nominal pore radius (0.4 μm), probably because vesicles are flexible and deform easily in such relatively large pores (this might not hold for smaller extrusion pores), or it can be due to minor differences between nominal and actual pore sizes. BSA-FITC-containing VETs resulted to be slightly larger than the other population, but this does not affect the overall conclusions of this study. VETs size distributions are truncated to the left at around 270-380 nm due to the combination of microscope resolution limit and reliability of automated image analysis. Note that CA-containing GVs have been instead extruded through polycarbonate membranes with larger pores (radius 1 μm) in order to collect large-enough VETs for a better determination of intra-vesicle fluorescence, which, in contrary to the other cases, is time-dependent (see Sections 2.3 and 5.3 for details). CA-containing VETs resulted to be smaller than the expected (and the population broader than expected) – see Table 1, last line – probably due to the fact that small vesicles can pass through the pores without being fragmented.

As in the GVs case, the internal solute concentration has been measured for each vesicle and plotted in Fig. 4 (bottom line). The distributions, in terms of solute concentration (y-axis) is again quite broad, and the dispersion of concentration around the mean increases as the size decreases (the average values are reported as green dashed lines in Fig. 4). This qualitatively fits with the expectations, as the smaller vesicles are expected to be highly

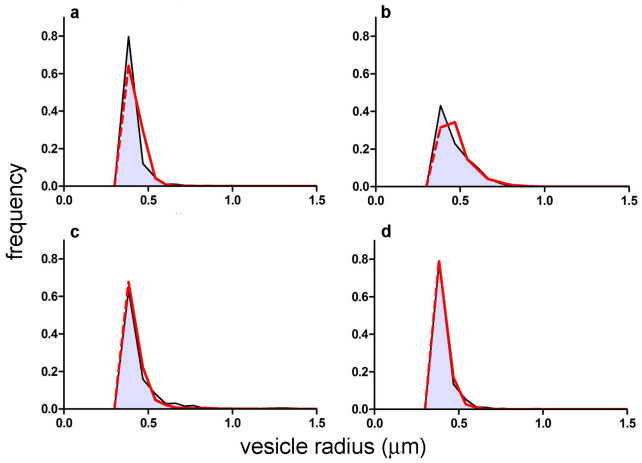

Fig. 5 Comparison between VETs size distribution as obtained experimentally (grey area) and by numerical modelling (negative exponential distribution, red curve). Size distributions refer to GVs filled with (a) pyranine; (b) calcein; (c) BSA-FITC; (d) dextran-FITC. Populations statistics are reported in Table 1. Note that both experimental and simulated size distributions (the latter being based on the exponential distribution) have been truncated at the resolution limit of microscope (a red dashed line has been added to the simulated exponential distribution just for the sake of comparison).

diverse with respect to the number of encapsulated solutes. Indeed the term $\sqrt{n}/n = 1/\sqrt{n}$ increases as the n decreases (n being proportional to the vesicle volume). From the quantitative viewpoint, however, also these intra-VETs solute distributions are broader than expected. The reason is that they originate from GVs which are already quite dispersed in terms of internal solute concentration.

When averaged over the whole VETs population, the mean solute concentrations in the case of pyranine, calcein, BSA-FITC, and dextran-FITC are 2.8 $\pm$ 0.7, 2.1 $\pm$ 1.4, 7.6 $\pm$ 1.0 and 0.55 $\pm$ 0.1 μM, respectively (Table 2). The comparison between such values and those referring to GVs (compare the dashed green and red lines in Fig. 4), shows that for pyranine and calcein there is a large concentration decrease, whereas for BSA-FITC and dextran-FITC there is a minor decrease. Solutes have been lost during extrusion. Note that the missing number of solute molecules mentioned here is not referring to the well-known volume loss when a large vesicle fragment into many small ones. The intra-VETs concentration is reduced because the local composition (per unit of volume) changes during the membrane rupture-and-resealing occurring during the vesicle extrusion.

2.2 Modelling

Intrigued by these observations, we set up a mathematical model that reproduces in all details the processes under investigation, asking whether the retention and the partition of solutes in the crucial moment of vesicle division (here substituted by forced extrusion through a narrow pore) follow theoretical expectations or not.

View Article Online
DOI: 10.1039/C7IB00138J

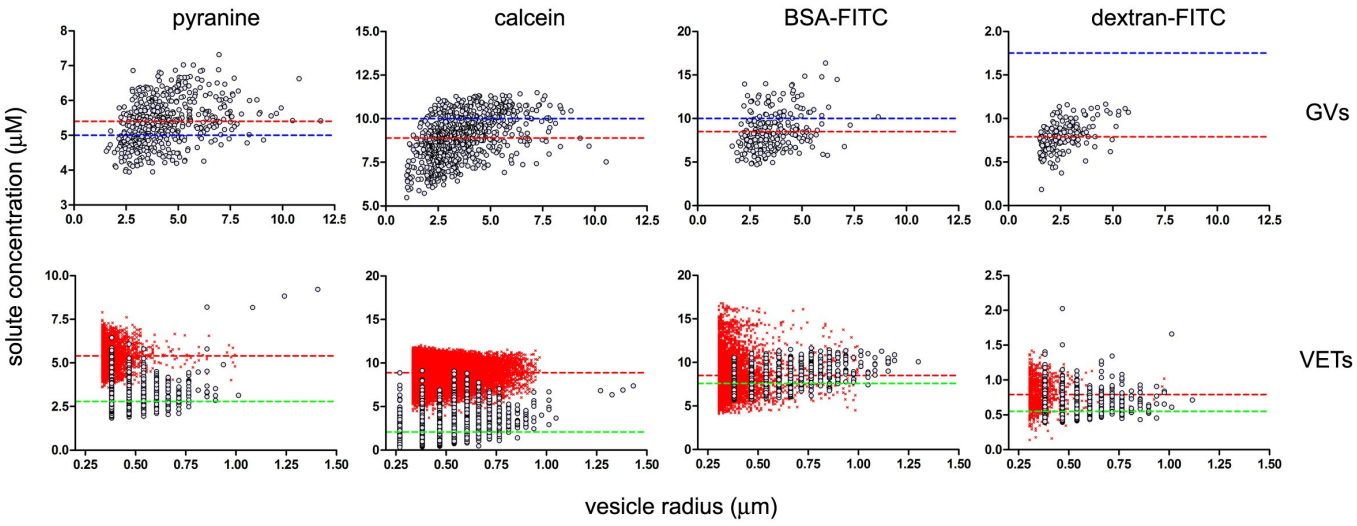

Fig. 4 Dependence of solute intra-vesicle concentration on vesicle radius given as bivariate dot-plots. GVs data are presented in the top line, VETs data in the bottom line; each column refer to a solute (pyranine, calcein, BSA-FITC, dextran-FITC). Experimental data indicated as grey circles; simulated data indicated as red crosses. In the four GVs plots on the top, the solute concentrations in bulk solution (referring to the solution used for GVs formation) are indicated by dashed blue lines (corresponding to 5, 10, 10 and 1.75 μM for the four above-mentioned solutes). The measured intra-GVs solute average concentration are instead reported as red dashed lines. For the four VETs plots on the bottom, the expected solute concentrations inside VETs (obtained after an 'ideal' extrusion) are indicated as red dashed lines (corresponding to the value found inside GVs, namely 5.4, 8.9, 8.5 and 0.79 μM). The average concentration values as obtained by the simulated extrusion are very close to these values (see Table 2). The measured intra-VETs average concentrations are indicated as green dashed lines (corresponding to 2.8, 2.1, 7.6 and 0.55 μM). The size cut-off in the case of VETs is due to the optical resolution limit.

2.2.1 *In silico* GVs

The starting point for modeling GVs extrusion is a GVs population generated *in silico* following a well-known model (the Helfrich distribution)[39] that fits rather well with the experimental data. The Helfrich distribution has as unique parameter R which is the average radius of the population. The resulting population $\omega(r)$, where r is the radius of the single vesicle, is given by:

$$\omega(r) = \frac{9r^3}{2R^4} exp\left(-\frac{3r^2}{2R^2}\right) \quad (1)$$

As shown in Fig. 3, there is an excellent agreement between the theoretical and experimental size distributions. The so-obtained *in silico* population of GVs was filled with solutes according to a Poisson process. The filling is the result of a pure stochastic process where the solute can accumulate randomly and without cooperative effects[15] or other kinds of inter-molecular interactions. Like the Helfrich's distribution, also the Poisson probability ($p(n) = e^{-\lambda}\lambda^n/n!$) depends on a single parameter which is the average value λ (n being the number of entrapped molecules). In our simulation λ has been set as the number of molecules expected in the GVS volume, according to $H_{0,I}$. The concentration of solutes inside GVs is equal, at least on average, to the solute concentration in the bulk (supposed uniform, as for a well-stirred environment). In other words, this is a simple space partition, that rules out any active contribution of the entrapment process. The Poisson process generates a random variability between the solute distribution in the *in silico* GVs (not shown). While this is a satisfactory procedure for pyranine-, calcein-, and BSA-FITC-containing GVs, it failed to model GVs prepared in the presence of dextran-FITC-containing GVs. For this reason, a new *in silico* GVs population has been produced by setting λ as the average number of dextran-FITC actually found in the vesicle's volume, *as determined experimentally* (0.79 μM instead of 1.75 μM). This was a mandatory change because in the next step (GVs extrusion) the starting point should be a GVs population that closely mimics the experimental data.

2.2.2 *In silico* VETs

In the next step, *in silico* solute-filled GVs were 'extruded' according to a stochastic algorithm. The unique constraints were that the emerging VETs size distribution should fit with the experimentally determined one (exponential distribution, truncated at the radius corresponding to the microscope resolution limit) and that the overall VETs membrane surface should be equal to the parent GVs membrane surface (i.e., the *in silico* extrusion process has no loss of lipids). The solutes contained in the parent GV were stochastically distributed in the daughter VETs (one GV generates several VETs) using a Poisson process, as in the previous step, and according to the second null hypothesis $H_{0,II}$ which simply states that the number of solute molecules is proportional to the vesicle volume.

The comparison between experimental and the simulated size distribution reveals again an excellent agreement (Fig. 5). The simulated intra-VETs solute concentrations are instead shown in Fig. 4 (bottom line). Here the small red crosses represent the expected concentrations of pyranine, calcein, BSA-FITC and dextran-FITC inside VETs. Their mean values are 5.4 $\pm$ 0.7, 9.0 $\pm$ 1.2, 8.6 $\pm$ 2.2, and 0.82 $\pm$ 0.20, respectively (Table 2). These values correspond to the expected values, namely the intra-GVs concentrations, in agreement with $H_{0,II}$. In other words, the GVs

View Article Online
DOI: 10.1039/C7IB00138J

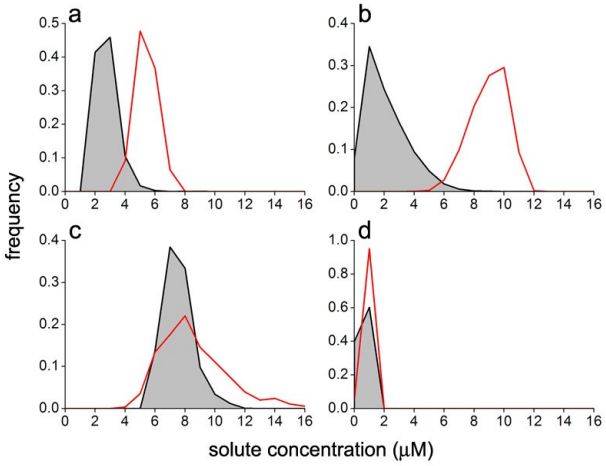

Fig. 6 Comparison between VETs solute occupancy distribution as obtained experimentally (grey area) and by numerical modelling (red lines). The distributions refer to VETs filled with (a) pyranine; (b) calcein; (c) BSA-FITC; (d) dextran-FITC. Note that the same concentration bins have been used for all cases. Populations statistics are reported in Table 2.

fragmentation, when carried out *in silico*, gives ideal VETs populations where the VETs have the same internal solute concentration of the parent GVs. However, intriguing discrepancies are found when the experimental and simulates values are compared (Table 2, Fig. 4 and Fig. 6). Low- and high-MW solutes behaves differently. The stochastic model has generated *in silico* populations of VETs that can be compared quantitatively with experimentally determined distributions and provides more information that a mere comparison among means. Fig. 6 shows such a comparison. It is evident that low-MW solutes (pyranine and calcein) are mainly lost during extrusion. In contrary, high molecular weight ones (BSA-FITC, dextran-FITC) are essentially retained.

2.3 The case of carbonic anhydrase

In addition to the four fluorescent solutes, we have studied the case of an enzyme entrapped in liposomes, aiming at modelling simple reactions occurring inside protocells. Carbonic anhydrase (CA) was employed, taking advantage of its esterase activity[36,37]. The non-fluorescent 6-carboxyfluorescein diacetate (CFDA) is a substrate of CA, which converts it in the fluorescent 6-carboxyfluorescein (CF), whose concentration can be monitored by confocal microscopy. CA-containing GVs were prepared as described; external CA is removed during GVs fractionation by centrifugation. GVs are then extruded in order to obtain CA-containing VETs. To start the reaction, CFDA is added to GVs or to VETs and the course of the enzymatic reaction is followed by measuring the green fluorescence which develops with time inside vesicles. Non-fluorescent CFDA penetrates into the vesicles' lumen by passive diffusion through the lipid membrane. Once inside, it is hydrolysed by CA to give the fluorescent product CF and acetate (Fig. 7).

The size distribution of CA-containing GVs resembles those obtained with the other solutes, but CA-containing VETs, being extruded through larger pores (radius 1 μm), are larger than the

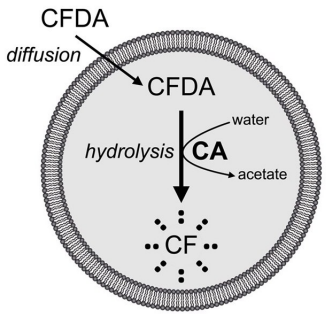

Fig. 7 Schematic drawing of CA-containing vesicles and their reaction with externally added CFDA. Fluorescent CF is produced after hydrolysis.

other cases, and their distribution is broader (see the bottom line of Table 1). The reason for this choice is that if the VETs are too small, it is difficult to measure the very weak intra-vesicle fluorescence that is generated in the initial period. This would result in a less reliable analysis. Starting from the experimental data, *in silico* CA-containing vesicles have been firstly generated using the Helfrich (GVs) and the exponential (VETs) functions to model their size distributions (not shown).

In order to proceed with the partition analysis, the intra-GVs CA concentration is required, but this value cannot be measured experimentally because CA does not fluoresce in the visible region. Thus, we elaborated a kinetic model for *calculating* the CA concentration inside vesicles. Each vesicle has been modelled as a CA-containing spherical microreactor with a semipermeable membrane. As a known amount of substrate CFDA is added to the vesicle suspension, it is possible to calculate the internal CF concentration, at any time and for any vesicle with radius r, by combining the CFDA passive diffusion equation and CA enzyme kinetics. Here, the reverse calculation is carried out, namely, determining the intra-vesicle CA concentration that leads to the measured CF concentration (details in Section 5.3). The model has been applied both to GVs and VETs. Such an approach allowed us to estimate, with a certain approximation, the intra-vesicle CA concentrations by a backward kinetic extrapolation.

Internal CA concentrations have been calculated after discrete time intervals from the addition of CFDA, up to 10 minutes. The average CA concentration inside GVs is 1.7 $\pm$ 1.0 μM. The mean value is below the bulk CA concentration used for the GVs preparation (2 μM), but the quite large variations among vesicles makes this difference not statistically significant. In turn, we ascribe the large standard deviation to the indirect determination of CA concentration, which is limited by the accuracy of r and CF fluorescence measurements. Using the experimental value (1.7 μM), the partition of CA has been simulated by creating firstly *in silico* GVs and then *in silico* VETs, as described above. Random and volume-based partition of CA in the daughter VETs, brings about a population with a mean CA concentration of 1.7 $\pm$ 0.3 μM. Such an *in silico* population was then compared with the experimental one, determined by calculating the CA content via the kinetic model. The intra-vesicle CA concentration results to be 1.0

View Article Online
DOI: 10.1039/C7IB00138J

Table 2 Average solute concentration (μM) inside VETs, mean $\pm$ s.d. The number of measured (or simulated) vesicles is indicated in parenthesis. The measured values of the last line, referring to CA-containing VETs has been calculate by a kinetic model, see Section 5, Eqs. 3-5. The Δ columns reports the difference between bulk, GVs, and VETs concentrations, as indicated. The percent reduction of intra-VET solute concentration, as measured after extrusion, is also shown on the last column. One asterisk marks statistical significance with respect to $H_{0,\mathrm{I}}$ or $H_{0,\mathrm{II}}$ (neat difference among the means); two asterisks mark statistical significance with respect to $h_{0,\mathrm{I}}$ or $h_{0,\mathrm{II}}$ (mean belonging or not to the parent distribution). For details, see Section 5.4 and Table 3.

Solute	Bulk	Intra-GVs (measured)	Δ(GVs$-$bulk)	Intra-VET (simulated)	Intra-VET (measured)	Δ(VETs$-$GVs)	normalized loss
pyranine	5	5.4 ± 0.7 (496)	$+0.4$*	5.4 ± 0.7 (4075)	2.8 ± 0.7 (4394)	-2.6**	-48%
calcein	10	8.9 ± 1.3 (814)	-1.1*	9.0 ± 1.2 (34299)	2.1 ± 1.4 (7554)	-6.8**	-76%
BSA-FITC	10	8.5 ± 2.1 (265)	-1.5*	8.6 ± 2.2 (6103)	7.6 ± 1.0 (4400)	-0.9*	-11%
dextran-FITC	1.75	0.79 ± 2.1 (179)	-0.96**	0.82 ± 0.20 (1191)	0.55 ± 0.11 (9634)	-0.24*	-30%
CA	2	1.7 ± 1.0 (233)	-0.3	1.7 ± 0.3 (4837)	1.0 ± 0.6 (368)	-0.7*	-41%

$\pm$ 0.6 μM. As for the other high-MW compounds, this comparison suggests that CA molecules are essentially retained during vesicle extrusion.

2.4 Solute occupancy distribution and 'super-filled' vesicles

One of the motivations of this study was the investigation of the possible formation of 'super-filled' vesicles from the fragmentation of larger mother vesicles. These special vesicles would derive from an uneven accumulation of solutes according to a specific mechanism. In this respect, it is useful to investigate in more detail the shape and the features of the solute concentration distributions, especially looking at their high-concentration tails. In the past, we have reported that under certain experimental conditions ferritin-[15] and ribosome-containing[40] conventional vesicles formed by natural swelling (25 nm $\leq r \leq$ 100 nm) display a power law distribution of the solute concentration.

In this study none of the investigated solutes has a power law occupancy distribution inside VETs. In particular, the distributions are all bell-shaped (Fig. 6). A small but measurable fraction of vesicles is however found on the high-concentration tail of the distributions. In particular, for the five solutes pyranine, calcein, BSA-FITC, dextran-FITC, and CA, the vesicles whose internal solute concentration is higher than the average concentration plus three standard deviations are 1.2%, 0.8%, 1.1%, 0%, and 0.6% of the whole population, respectively (*cf.* with the expected 0.3% of a Gaussian distribution).

3 Discussion

The two processes depicted in Fig. 1 have been scrutinized against four null hypotheses, $H_{0,\mathrm{I}}$ and $h_{0,\mathrm{I}}$ for the vesicle formation step/solute encapsulation, and $H_{0,\mathrm{II}}$ and $h_{0,\mathrm{II}}$ for the vesicle extrusion step/solute partition. Table 2 summarizes the results of such analysis (statistical details in Section 5.4 and Table 3).

3.1 Process 1. Vesicle formation and solute entrapment

When the difference between C_{bulk} and $\langle C_{\mathrm{GVs}} \rangle$ is strictly considered, it results that $H_{0,\mathrm{I}}$ should be rejected for all solutes but CA (this latter result, probably, derives from the quite broad intra-GVs solute concentration distribution, which has been obtained by numerical methods, rather than to a true qualitatively different behaviour). A large difference, however, is observed only in the case of dextran-FITC, where in addition to $H_{0,\mathrm{I}}$ also $h_{0,\mathrm{I}}$ is rejected. This is well evident in Fig. 4 where a large distance between the blue and red dashed lines is present only in the dextran-FITC panel. The reduced entrapment efficiency for high-MW dextran was already observed[41]. The average values of intra-GVs concentrations of pyranin and calcein, both negatively charged at the experimental pH, are unexpectedly above and below the corresponding C_{bulk}, suggesting either fine-tuned molecular effects either a very cautious use of average values, also in view of the sample high dispersity. Our results suggest that sampling a vesicle population to obtain an average behaviour is *per se* not a trivial process, due to the very heterogeneous nature of vesicle samples (when prepared by the natural swelling) and that the concept of mean concentration should be utilized cautiously. The encapsulation of macromolecules, and in particular of proteins (enzymes) is know to be dependent on several factors, as the operative procedure, pH, ionic strength, and the nature of lipids[42–44]. Here we have shown that working on similar conditions, MW plays a major role in encapsulation. With respect to dispersion around the mean value, it is well known, but not studied in detail, that the formation of vesicles brings about a heterogeneous population in terms of solute content. A previous report indicates that 5-20 kDa poly(ethylene glycol)- and 4-2,000 kDa dextran-containing GVs prepared by the natural swelling method have solute distribution widths of $\pm$ 50% around the average concentration[41]. Numerous flow cytometry studies[28,29,45] carried out on GVs prepared both by the natural swelling method and by droplet transfer have also evidence similar trends. Here we have shown that, for GVs prepared by the natural swelling method, and for all investigated solutes, such a GVs heterogeneity (or 'diversity'[46]) is normally present, and that it is higher than expected. The physics behind the large dispersion around the mean concentration value is not well known and should be investigated separately for each preparation method.

3.2 Process 2. Vesicle division (here, fragmentation) simulated by extrusion

We have inquired on what happen to encapsulated solutes during extrusion – intended as an artificial model of vesicle division. This is an important point as the small vesicles deriving from division (or fragmentation) of a parent one must inherit the solutes therein contained, in order to be able performing similar functions (imagine the fragmentation of primitive cells containing dozens of different molecular species). In the past, the fate of solutes during vesicle self-reproduction was firstly studied by

View Article Online
DOI: 10.1039/C7IB00138J

employing ferritin-containing oleic acid/oleate vesicles (radius of about 45 nm), which spontaneously undergo self-reproduction when fed with oleate micelles[19,20]. The daughter vesicles (ca. 30 nm) contained ferritin with a similar distribution of the parent one, but the average ferritin number inside the daughter vesicles was less than the initial value due to the co-presence of several new empty vesicles. Subsequent studies showed that the extrusion of calcein-containing myristoleate vesicles (radius reduction from 70 to 44 nm) brings about a calcein loss (−55%) that could not be explained by the decrease of the vesicle volume (−38%)[38]. The spontaneous division of lecithin-stabilized water-in-oil droplets (3.5 μm) wherein the green fluorescent protein was being produced let to smaller droplets (ca. 2 μm) without interruption of protein synthesis[22]. Here we have studied the solute partition pattern following the extrusion of GVs (radius around 3.5 μm) to 0.4 μm VETs in the presence of encapsulated low- and high-MW solutes. With respect to the previous studies, which focused on small volume reduction, the volume difference among GVs and VETs volume is remarkable. It is expected that the extrusion of one GVs typically yields 70-80 VETs, and about 90% of GVs content is lost. We investigated whether the remaining 10% is homogeneously partitioned in the daughter VETs or not. The last two columns of Table 2 show absolute and relative differences between intra-VETs and intra-GVs solute concentrations. All differences are statistically significant (i.e., $H_{0,\mathrm{II}}$ must be rejected for all solutes). However, when the less restrictive $h_{0,\mathrm{II}}$ is considered, the solute retention appears to be a function of MW ($h_{0,\mathrm{II}}$ is rejected only for pyranine and calcein). Pyranine and calcein are largely released during GVs extrusion, and the intra-VETs solution results sensitively different (solute-depleted) when compared to GVs one. Vice versa, macromolecules like BSA, dextran and CA (the latter at a minor extent) appear to be less sensitive to solute loss during extrusion, and are therefore more retained than low-MW solutes. The last column of Table 2 indicates the percent decrease of intra-VETs solute concentration. Pyranine and calcein show high solute loss (−48-76%), whereas the corresponding values for BSA-FITC, dextran-FITC and CA lies in the −11-41% range. These trends partially overlap, also considering inter-experiment reproducibility ($\sim$ 5%), but reveal an interesting and potentially important effect that deserves further attention.

3.3 Physical mechanism

As mentioned, vesicle extrusion consists in the forced passage of large vesicles through narrow channels of a thin polycarbonate sheet[47]. The vesicle membrane is deformed when it enters in the channel, forced by the pressure exerted above the membrane, and fragments into smaller vesicles with diameters approximately equal to the diameter of the pore. The effect of applied pressure on the size of extruded vesicles has been studied in details for a number of pore size (up to diameters of 200 nm), lipids, concentrations, and temperatures[48–50]. In particular, it has been shown that the a threshold pressure should be overcome to extrude vesicles, and that vesicle size inversely depends on the square root of applied pressure (see also a short discussion on the pressure exerted for extruding GVs in this study in Section 5.2.1). The mechanism of vesicle formation is not well understood, but it is clear that the membrane of the mother vesicle must break, and only afterword its membrane fragments reseal to form new small vesicles. Whether this occurs via an extended membrane fragmentation (and then resealing) or budding of small membrane portions[48,49,51] it is evident that solutes can escape from the broken mother compartment before ending (re-captured) in the *in situ*-formed smaller vesicles. In absence of strong solute-membrane interaction, the fate of solutes will be determined essentially by their diffusion coefficient D, which depends on molecular size and shape. Considering the solutes under study as spherical particles, D is estimated to be around 500 μm^2/s (low-MW) and 100 μm^2/s (high-MW) by the Stokes-Einstein relation. The three-dimensional mean displacement ρ of these solutes in the typical time required to vesicle closure (ca. 1 ms)[52] is 1.73 μm (low-MW) and 0.77 μm (high-MW), calculated according to Eq. 2

$$\rho = \sqrt{6Dt} \tag{2}$$

Thus, considering that VETs have typical diameters of 0.8 μm (or ca. 1.5 μm in the case of CA-containing vesicles), small molecules have lower chances to be entrapped inside the incipient vesicles, whereas for macromolecules the opposite is true. Although this analysis does not allow the discrimination between the two possible extrusion mechanisms, it identifies molecular size and thus diffusion as the primary factors that explain the observations.

It is interesting to note – at least for pyranine, calcein, BSA-FITC and dextran-FITC cases – that the VETs mean sizes and dispersions around the mean are comparable (see Table 1), suggesting that the extrusion of these four different samples occurred at similar pressure (and plausibly quite low, of the order of few bars). This implies that the mechanisms underlying the extrusion of solute-filled GVs, in the four above-mentioned cases, was not dramatically different. In fact, previous studies have shown that vesicle mean size depends on applied extrusion pressure (but accurate measurements have been carried out only for membrane pores of diameter 200 nm, or smaller)[48–50]. Moreover, there is no correlation between mean VET size and solute retention, implying that even if minor pressure differences were applied for extruding these samples, this did not invalidate the conclusions of this study. Such considerations allow us to conclude that the observed variations of intra-vesicle solute concentrations are due to solute size, and not to different mechanism of membrane breakage and resealing. Unfortunately, CA-containing VETs cannot be directly compared with the other cases, because they have been extruded through membrane with larger pores.

4 Concluding remarks

Although this work has shown an interesting tendency, *i.e.*, that macromolecules could be preferentially retained inside daughter vesicles derived from fragmentation (and, by extrapolation, from division) of a mother vesicle, it should not be considered conclusive. There are several open questions not covered by our investigation. The first one is whether the observed behaviour is really

View Article Online
DOI: 10.1039/C7IB00138J

general or it can be observed only for the five types of solutes studied here. This knowledge gap should be covered by extending such kind of study on many more low- and high-MW solutes, including nucleic acids for instance. Second, POPC GVs have been used as protocellular models, but other kind of membranes should be explored. In the field of phospholipids, an interesting question refers to changing the chain length (*e.g.*, DMPC) or the membrane fluidity (*e.g.*, DOPC, POPC, DPPC and their mixtures), as well as the effect of cholesterol. Maybe more importantly, fatty acid vesicles, which are generally considered realistic protocell models[53], should be investigated. Third, it should be kept in mind that our results are based on a mechanical fragmentation, whereas the final goal refers to spontaneous vesicle division, following a growth-division mechanism[4–6]. A more stringent control of extrusion pressure, is however required to corroborate our observations. Thus, we hope for future studies that address all these aspects.

At the aim of extending the relevance of our study also outside origin-of-life research, we noted that the physical mechanisms at the basis of VETs formation from GVs could be of interest for research on exosomes[54–56]. In particular, it is an open question whether physical factors could act in synergy with highly regulated control bio-mechanisms operating when exosomes stem from large cells. In this respect it should also mentioned that recently reported 'super-filled' vesicles, whose diameter lies in the 60-200 nm range, [15,40] can be considered intriguing models of exosomes, as they contain closely packed biomacromolecules (proteins, ribosomes).

Returning to an origin-of-life scenario, this study suggests - albeit with the due caution - that very basic biophysical mechanisms (based on solute size) could have been a source of selective pressure in prebiotic times, before the onset of sophisticated control mechanism of cell reproduction, favouring the vertical transfer of macromolecules (information-carrying and/or catalytic polymers) through generations of primitive cells.

5 Materials and Methods

5.1 Materials

8-Hydroxypyrene-1,3,6-trisulfonic acid trisodium salt (pyranine, #H1529, 524 Da), calcein disodium salt (#21030, 667 Da), bovine serum albumin-fluorescein isothiocyanate conjugate (BSA-FITC, #A9771, 66 kDa), dextran-fluorescein isothiocyanate conjugate (dextran-FITC, #FD150S, 150 kDa), carbonic anhydrase (CA, #C4396, 60 kDa), and 6-carboxyfluorescein diacetate (CFDA, #C5041, 460 Da) were all from Sigma-Aldrich, as well as all solvents and buffers used in the study. POPC (1-palmitoyl-2-oleoyl-*sn*-glycero-3-phosphatidylcholine) was bought from Avanti (Alabaster, AL, USA). DMSO stands for dimethyl sulfoxide.

5.2 Methods

Preliminary tests and optimizations showed good inter-experiment reproducibility (average values within ∼5%) provided that extensive vesicle sampling is carried out.

5.2.1 Preparation of vesicles

Giant vesicles (GVs) have been prepared by the natural swelling method. POPC films were prepared in round-bottom cylindrical glass vials (diameter ca. 2 cm) by introducing 2.5 μmol POPC (as chloroform solution) and removing the solvent at about 15 mbar by a Rotavapor (Büchi). Residual solvent was removed at 1 mbar. The lipid film was gently hydrated for about 14 hours at 25 °C, with 1.0 mL of hydration buffer (200 mM sucrose, 5 mM Na-bicine pH 8.5), without any mechanical stirring. The hydration buffer also contained a known amount of the solute that need to be encapsulated inside GVs. The resulting GVs sample ([POPC] = 2.5 mM) was then treated as described below. Five different GVs samples were obtained by including in the hydration buffer, respectively, 5 μM pyranine, 10 μM calcein, 10 μM BSA-FITC, and 1.75 μM dextran-FITC.
In order to separate GVs from non-entrapped solutes and isolate small-sized GVs, 3 volumes of GVs were diluted with 1 volume of dilution buffer (200 mM glucose, 5 mM Na-bicine pH 8.5). This creates an isotonic density gradient that allows a facile GVs centrifugation. The raw GVs samples were centrifuged and washed at increasing rates (700, 1,000 and 5,000 rpm on a Eppendorf desktop centrifuge). The final GVs pellet was suspended in 200 μL of working buffer (150 mM sucrose, 50 mM glucose, 5 mM Na-bicine pH 8.5). Due to material loss during the centrifugation procedure, it was convenient to prepare a large volume of GVs (4 × 1 mL). The final POPC concentration was 1.1 mM as estimated by the Stewart assay[57]. The centrifugation allows the removal of non-entrapped solutes and brings about the isolation of GVs whose radius lies in the 1-10 μm range.
Solute-containing GVs (0.5 mL) were extruded (seven passages) in order to prepare sub-micrometer extruded vesicles with nominal radius of 0.4 μm (Vesicles by the Extrusion Technique, VETs). Extrusion was carried out by means of a hand-extruder (Liposofast, Avestin, Canada), whereby two 0.4 μm-pores (radius) polycarbonate membranes (Corning Nuclepore Track-Etch Membranes) were sandwiched between three support drain discs. In the case of CA-containing vesicles, membranes with 1 μm-pores (nominal radius) have been used.

It is known that the radius of extruded vesicles tend to the radius of extrusion pores as the exerted pressure increases[50]. However, as the membrane pore diameter (0.8 or 2 μm) used in this study is quite larger when compared with the case of well-studied extrusion on pores whose diameter is 200 nm or less[48–50], available knowledge does not allow a quantitative discussion on the effect of pressure on extrusion. A tentative approach can be based on the following considerations. According to the available hand-extruder technical specifications (from Genizer, San Gabriel, CA), the maximal pressure that can be exerted on the hand-extruder is ca. 150 psi (ca. 10 bar), whereas the minimal pressure for extrusion of 1.1 mM POPC through 800 nm (diameter) pores it is difficult to estimate (*cf.* the threshold pressure for extruding 0.13 mM POPC vesicles on 100 nm (diameter) pores is ca. 2.8 bar[50]). Thus, even if the extrusion pressure has not been controlled in this study, it realistically lies in the 3-10 bar range. However, as the mean

View Article Online
DOI: 10.1039/C7IB00138J

VET sizes, and the dispersions around the mean are very similar (see Table 1), it can be cautiously concluded that the occasional pressure variations unavoidably associated to hand extrusion have not been decisive to determine different vesicle sizes and different vesicle extrusion mechanisms.

5.2.2 Enzyme reaction inside vesicles

CA-containing GVs were prepared, purified and extruded as described above, but 5 mM Na-bicine pH 8.5 was substituted by 5 mM Tris-HCl pH 7.5. CA concentration in the hydration buffer was 2 μM. In order to start the reaction, CA-containing vesicles (GVs or VETs) were treated with 400 μM CFDA (added as DMSO solution; the final DMSO concentration was 3% v/v). Non-fluorescent CFDA permeates inside vesicles where it is hydrolysed by CA[36,37], giving the fluorescent product carboxyfluorescein (CF), which stays entrapped in the vesicle.

The Michaelis-Menten parameters of the CA-catalysed CFDA-hydrolysis were determined for the reaction in bulk by adding 13 to 665 μM CFDA (final DMSO concentration was kept constant at 5% v/v) to 1 μM CA in 200 mM sucrose, 5 mM Tris-HCl (pH 7.5) and measuring the initial reaction rate by recording the absorbance at 491 nm, where the product of the reaction, CF, has an absorption peak (ε_{491} = 61,300 cm^{-1} M^{-1}, measured at pH 7.5). The apparent turnover number ($k_{\rm cat}$) and the apparent Michaelis-Menten constant ($K_{\rm M}$) have been determined by non-linear and linear fittings of experimental data, giving consistently the values of 3.0 $\pm$ 0.2 s^{-1} and 4.0 $\pm$ 0.3 mM, respectively.[17]

5.2.3 Vesicle observation and image analysis

Vesicles observation by confocal laser scanning microscopy and image acquisition. GVs and VETs have been observed by means of a Leica TCS SP5 confocal microscope. Images were acquired at 1024 $\times$ 1024 resolution, 8-bit depth. All fluorochromes used in this study can be excited by the 488 nm Argon laser line; fluorescence was collected in the 500-550 nm range. Vesicles (30 μL) have been diluted with 70 μL of isotonic isopycnic buffer (150 mM sucrose; 50 mM glucose; and 5 mM Na-bicine pH 8.5 or 5 mM Tris-HCl pH 7.5) and directly visualized without any pretreatment. Visualization chambers have been created by overlapping a microscope glass slide and a 0.17 mm cover slip above each other, using as a spacer two layers of properly shaped and molten Parafilm M (which holds together the glass slide and the cover slip). Due to the complete removal of non-entrapped solutes, GVs background was not fluorescent, whereas VETs background was partly fluorescent, as expected, because of solute loss during GVs extrusion. In the case of CA-containing vesicles, CFDA (as DMSO solution) was added to the vesicle sample and thoroughly mixed just before placing the sample in the visualization chamber; images were recorded at regular time intervals, for a total time of 40 minutes.

Image analysis. Quantitative image analysis was carried out by using ImageJ (http://imagej.nih.gov/ij). The background average fluorescence (F_0) and standard deviation (ΔF) of the 8-bit green-channel images were firstly measured, in order to set the threshold at the $F_0 + 3\Delta F$ fluorescence value. In the resulting 1-bit images, the vesicles were recognized by the built-in ImageJ algorithm. The ROIs map was then applied to the original 8-bit images and vesicle parameters were measured (projected area, fluorescence, shape). Shape descriptors (circularity and solidity) were used to discard bad-quality vesicles. Vesicle projected areas have been assumed to be the vesicle great circle, and from this, vesicle radius was calculated. This assumption is accurate for VETs but can lead to GVs size underestimation (because the confocal optical slice in our experimental conditions is about 0.7 μm). Intra-vesicle fluorescence values were converted to solute concentrations by means of calibration lines. Care was taken to image free-solute samples at the same optical depth (along the z-direction) of the vesicle samples.

5.3 Kinetic analysis of CA-catalyzed CFDA hydrolysis

The external addition of CFDA to CA-containing spherical unilamellar vesicles of radius triggers two processes, namely, the passive diffusion of CFDA from the external solution to the vesicle lumen, and its CA-catalysed hydrolysis to give CF and acetate. In order to model these processes the required physico-chemical parameters are the CFDA permeability coefficient across the phosphatidylcholine membrane[58] ($\wp = 10^{-7}$ cm/s), and the CFDA/CA Michaelis-Menten kinetic parameters ($k_{\rm cat}$ and $K_{\rm M}$).

Given the vesicle radius r, the initial external CFDA concentration $[\mathrm{CFDA}]_{0,\mathrm{out}}$ and the intra-vesicle CA concentration $\mathrm{E_{in}}$ (which is supposed not to change in time), it is possible to calculate, under certain approximations and by numerical integration, the internal CF concentration at any time $[\mathrm{CF}]_{t,\mathrm{in}}$. Similarly, it is possible to carry out the inverse calculation, namely determining $[\mathrm{CA}]_{\mathrm{in}}$ from r, $[\mathrm{CFDA}]_{0,\mathrm{out}}$, and $[\mathrm{CF}]_{t,\mathrm{in}}$. The reaction can be summarized as it follows:

$$\mathrm{CFDA_{out}} \underset{\text{efflux}}{\overset{\text{influx}}{\rightleftharpoons}} \mathrm{CFDA_{in}} \xrightarrow[\text{hydrolysis}]{\text{CA}} \mathrm{CF_{in}}$$

The time evolution of all species has been obtained by numerical integration of the ordinary differential equations 3-5:

$$\frac{d[\mathrm{CFDA}]_{t,\mathrm{out}}}{dt} = -\frac{\sigma_{\mathrm{ves}}}{V_{\mathrm{ext}}}\wp\left([\mathrm{CFDA}]_{t,\mathrm{out}} - [\mathrm{CFDA}]_{t,\mathrm{in}}\right) \quad (3)$$

$$\frac{d[\mathrm{CFDA}]_{t,\mathrm{in}}}{dt} = \frac{\sigma_{\mathrm{ves}}}{V_{\mathrm{ves}}}\wp\left([\mathrm{CFDA}]_{t,\mathrm{out}} - [\mathrm{CFDA}]_{t,\mathrm{in}}\right) - -k_{\mathrm{cat}}\frac{\mathrm{E_{in}}[\mathrm{CFDA}]_{t,\mathrm{in}}}{K_{\mathrm{M}} + [\mathrm{CFDA}]_{t,\mathrm{in}}} \quad (4)$$

$$\frac{d[\mathrm{CF}]_{t,\mathrm{in}}}{dt} = k_{\mathrm{cat}}\frac{\mathrm{E_{in}}[\mathrm{CFDA}]_{t,\mathrm{in}}}{K_{\mathrm{M}} + [\mathrm{CFDA}]_{t,\mathrm{in}}} \quad (5)$$

where σ_{ves}, V_{ves}, and V_{ext} are, respectively, the vesicle surface, the vesicle volume, and the external volume; $\wp$ is the CFDA permeability through the lipid bilayer. In order to determine the unknown enzyme concentration inside the vesicles ($\mathrm{E_{in}}$), the evolution of the product concentration $[\mathrm{CF}]_{t,\mathrm{in}}$ (whose value was recorded by confocal microscopy after at known amounts of time t_{m}) was simulated by the numerical solution of Equations 3-5 for each measured vesicles. In particular, $\mathrm{E_{in}}$ was varied by a binary search approach until the difference between the experimental

View Article Online
DOI: 10.1039/C7IB00138J

and calculated $[CF]_{t_m,in}$ was less than the desired accuracy $\varepsilon = 10^{-6}$ μM. Note that a numerical solution was found for the majority of vesicles, however in some cases the routine did not converge.

5.4 Statistical analysis

Statistical tests were applied to draw conclusions with respect to the hypotheses under scrutiny. For all tests, statistical significance was attributed when $p < 0.05$. In addition to $H_{0,I}$ and $H_{0,II}$, specified at the beginning of Section 2, the following hypotheses were also statistically tested:

$h_{0,I}$, that C_{bulk} belongs to the population of intra-GVs concentrations; i.e., $C_{bulk} \in \{C_{GVs}\}$;

$h_{0,II}$, that $\langle C_{VETs} \rangle$ belongs to the population of intra-GVs concentrations; i.e., $\langle C_{VETs} \rangle \in \{C_{GVs}\}$;

where C_{bulk}, $\langle C_{VETs} \rangle$, and $\{C_{GVs}\}$ represent, respectively, the solute bulk concentration in the solution used to form GVs, the average intra-VETs solute concentration, and the whole population of intra-GVs solute concentration.

The normality of the GVs and VETs solute occupancy distribution (internal solute concentration, μM) was assessed by the Kolmogorov-Smirnov test, as reported in Table 3, entries 1 and 2. Similar but not identical conclusions were obtained by the Shapiro-Wilk W-test and by the Lilliefors test (only pyranine- and calcein-containing GVs gave contrasting results). $H_{0,I}$ compares an individual value with a mean, and it was assessed by a one-sample t-test (two-tailed). $H_{0,II}$ compares two means that derive from two non-normal populations, and it was assessed by the Mann-Whitney nonparametric test (two-tiled). The two additional hypotheses $h_{0,I}$ and $h_{0,II}$ compare an individual value with a population (i.e., with a distribution function, which is non necessarily normal). In order to proceed, the experimental distribution was best-fitted to give either a normal distribution (when the normality test was passed) or a log-normal distribution (when the normality test was not passed); the resulting probability density function was used to compute the p-value (one-tailed).

5.5 *In silico* GVs and VETs, and solute partition

The simulations of GVs and VETs size and solutes distributions were performed by using lab-made Python routines. In particular, pseudo-random number generations and Poisson random variables where managed thanks to `Numpy` and `MatPlotLib` open source scientific libraries. Due to the very large number of substrate molecules involved, the dynamical simulation of CA reaction has been implemented in a deterministic way, by calculating the standard Michaelis-Menten enzyme kinetics.

Acknowledgements

The authors are grateful to Pier Luisi Luisi (ETH Zürich, Switzerland and Roma Tre University, Italy) for inspiring discussions on the open questions about vesicle roles in primitive origins-of-life scenarios. Collaboration among the authors has been fostered by the European COST Action CM1304 "Emergence and Evolution of Complex Chemical Systems".

References

1 P. L. Luisi, F. Ferri and P. Stano, *Naturwissenschaften*, 2006, **93**, 1–13.
2 V. de Lorenzo and A. Danchin, *EMBO reports*, 2008, **9**, 822–827.
3 J. C. Blain and J. W. Szostak, *Annual Review of Biochemistry*, 2014, **83**, 615–640.
4 P. Walde, R. Wick, M. Fresta, A. Mangone and P. Luisi, *Journal of the American Chemical Society*, 1994, **116**, 11649–11654.
5 P. Stano, E. Wehrli and P. L. Luisi, *Journal of Physics: Condensed Matter*, 2006, **18**, S2231.
6 T. F. Zhu and J. W. Szostak, *Journal of the American Chemical Society*, 2009, **131**, 5705–5713.
7 W. Yu, K. Sato, M. Wakabayashi, T. Nakaishi, E. P. Ko-Mitamura, Y. Shima, I. Urabe and T. Yomo, *Journal of bioscience and bioengineering*, 2001, **92**, 590–593.
8 S. Nomura, K. Tsumoto, T. Hamada, K. Akiyoshi, Y. Nakatani and K. Yoshikawa, *Chembiochem*, 2003, **4**, 1172–1175.
9 V. Noireaux and A. Libchaber, *Proceedings of the National Academy of Sciences of the United States of America*, 2004, **101**, 17669–17674.
10 G. Murtas, Y. Kuruma, P. Bianchini, A. Diaspro and P. L. Luisi, *Biochemical and biophysical research communications*, 2007, **363**, 12–17.
11 Y. Kuruma, P. Stano, T. Ueda and P. L. Luisi, *Biochimica et biophysica acta*, 2009, **1788**, 567–574.
12 G. Sessa and G. Weissmann, *Journal of Biological Chemistry*, 1970, **245**, 3295–3301.
13 D. W. Deamer and G. L. Barchfeld, *Journal of molecular evolution*, 1982, **18**, 203–206.
14 P. Walde and S. Ichikawa, *Biomolecular engineering*, 2001, **18**, 143–177.
15 P. L. Luisi, M. Allegretti, T. P. de Souza, F. Steiniger, A. Fahr and P. Stano, *Chembiochem*, 2010, **11**, 1989–1992.
16 P. Stano, E. D'Aguanno, J. Bolz, A. Fahr and P. L. Luisi, *Angewandte Chemie International Edition*, 2013, **52**, 13397–13400.
17 E. D'Aguanno, E. Altamura, F. Mavelli, A. Fahr, P. Stano and P. L. Luisi, *Life*, 2015, **5**, 969–996.
18 F. Mavelli and P. Stano, *Artif. Life*, 2015, **21**, 445–463.
19 N. Berclaz, M. Müller, P. Walde and P. L. Luisi, *Journal of Physical Chemistry B*, 2001, **105**, 1056–1064.
20 N. Berclaz, E. Blöchliger, M. Müller and P. L. Luisi, *Journal of Physical Chemistry B*, 2001, **105**, 1065–1071.
21 M. M. Hanczyc, S. M. Fujikawa and J. W. Szostak, *Science (New York, N.Y.)*, 2003, **302**, 618–622.
22 D. Fiordemondo and P. Stano, *Chembiochem: A European Journal of Chemical Biology*, 2007, **8**, 1965–1973.
23 F. Mavelli, *BMC Bioinformatics*, 2012, **13 Suppl 4**, S10.
24 Y. P. Patil, A. K. Ahluwalia and S. Jadhav, *Chem. Phys. Lipids*, 2013, **167-168**, 1–8.
25 P. Walde, R. Wick, M. Fresta, A. Mangone and P. Luisi, *Journal of the American Chemical Society*, 1994, **116**, 11649–11654.
26 P. Stano and P. L. Luisi, *Chemical communications (Cambridge,*

View Article Online
DOI: 10.1039/C7IB00138J

Table 3 Table of *p*-values as resulted from the statistical analysis of the experimental values. Statistical significance ($p < 0.05$) is marked with an asterisk. Details are given in Section 5.4.

#	Hypotheses under scrutiny	pyranine	calcein	BSA-FITC	dextran-FITC	CA
1	Normality of intra-GVs solute distribution	> 0.20	< 0.10	< 0.01*	> 0.20	< 0.01*
2	Normality of intra-VETs solute distribution	< 0.001*	< 0.001*	< 0.001*	< 0.001*	< 0.001*
3	$H_{0,\mathrm{I}}$, i.e., $C_{\mathrm{bulk}} = \langle C_{\mathrm{GVs}} \rangle$	< 0.001*	< 0.001*	< 0.001*	< 0.001*	0.3848
4	$h_{0,\mathrm{I}}$, i.e., $C_{\mathrm{bulk}} \in \{C_{\mathrm{GVs}}\}$	0.692	0.204	0.211	< 0.001*	0.248
5	$H_{0,\mathrm{II}}$, i.e., $\langle C_{\mathrm{VETs}} \rangle = \langle C_{\mathrm{GVs}} \rangle$	< 0.001*	< 0.001*	< 0.001*	< 0.001*	< 0.001*
6	$h_{0,\mathrm{II}}$, i.e., $\langle C_{\mathrm{VETs}} \rangle \in \{C_{\mathrm{GVs}}\}$	< 0.001*	< 0.001*	0.628	0.081	0.486

England), 2010, **46**, 3639–3653.

27 K. Kurihara, M. Tamura, K.-I. Shohda, T. Toyota, K. Suzuki and T. Sugawara, *Nature chemistry*, 2011, **3**, 775–781.

28 T. Sunami, K. Sato, T. Matsuura, K. Tsukada, I. Urabe and T. Yomo, *Analytical Biochemistry*, 2006, **357**, 128–136.

29 K. Nishimura, T. Hosoi, T. Sunami, T. Toyota, M. Fujinami, K. Oguma, T. Matsuura, H. Suzuki and T. Yomo, *Langmuir*, 2009, **25**, 10439–10443.

30 L. Lazzerini-Ospri, P. Stano, P. Luisi and R. Marangoni, *Bmc Bioinformatics*, 2012, **13**, S9.

31 K. Nishimura, T. Matsuura, K. Nishimura, T. Sunami, H. Suzuki and T. Yomo, *Langmuir*, 2012, **28**, 8426–8432.

32 L. Calviello, P. Stano, F. Mavelli, P. L. Luisi and R. Marangoni, *BMC Bioinformatics*, 2013, **14**, S7.

33 E. Altamura, F. Milano, R. R. Tangorra, M. Trotta, O. H. Omar, P. Stano and F. Mavelli, *Proceedings of the National Academy of Sciences of the United States of America*, 2017, **114**, 3837–3842.

34 A. C. Chakrabarti, R. R. Breaker, G. F. Joyce and D. W. Deamer, *Journal of molecular evolution*, 1994, **39**, 555–559.

35 P. A. Monnard and D. W. Deamer, *Origins of life and evolution of the biosphere: the journal of the International Society for the Study of the Origin of Life*, 2001, **31**, 147–155.

36 R. E. Tashian, D. P. Douglas and Y. S. Yu, *Biochem. Biophys. Res. Commun.*, 1964, **14**, 256–261.

37 J. A. Verpoorte, S. Mehta and J. T. Edsall, *J. Biol. Chem.*, 1967, **242**, 4221–4229.

38 M. M. Hanczyc, S. M. Fujikawa and J. W. Szostak, *Science*, 2003, **302**, 618–622.

39 W. Helfrich, *Journal de Physique*, 1986, **47**, 321–329.

40 T. Pereira de Souza, F. Steiniger, P. Stano, A. Fahr and P. L. Luisi, *Chembiochem*, 2011, **12**, 2325–2330.

41 L. M. Dominak and C. D. Keating, *Langmuir*, 2007, **23**, 7148–7154.

42 R. L. Shew and D. W. Deamer, *Biochim. Biophys. Acta*, 1985, **816**, 1–8.

43 J.-P. Colletier, B. Chaize, M. Winterhalter and D. Fournier, *BMC Biotechnol.*, 2002, **2**, 9.

44 S. Y. Hwang, H. K. Kim, J. Choo, G. H. Seong, T. B. D. Hien and E. K. Lee, *Colloids Surf B Biointerfaces*, 2012, **94**, 296–303.

45 T. Sakakura, K. Nishimura, H. Suzuki and T. Yomo, *Anal. Methods*, 2012, **4**, 1648–1655.

46 P. Stano, T. Souza, P. Carrara, E. Altamura, E. D'Aguanno, M. Caputo, P. L. Luisi and F. Mavelli, *Mechanics of Advanced Materials and Structures*, 2015, **22**, 748–759.

47 P. Walde, *Encyclopedia of Nanoscience and Nanotechnology*, H. S. Nalwa (Ed.), American Scientific Publishers edn, 2004, vol. 9, pp. 43–79.

48 D. G. Hunter and B. J. Frisken, *Biophys. J.*, 1998, **74**, 2996–3002.

49 B. J. Frisken, C. Asman and P. J. Patty, *Langmuir*, 2000, **16**, 928–933.

50 P. J. Patty and B. J. Frisken, *Biophysical Journal*, 2003, **85**, 996–1004.

51 S. G. Clerc and T. E. Thompson, *Biophys. J.*, 1994, **67**, 475–476.

52 E. Hernández-Zapata, L. Martínez-Balbuena and I. Santamaría-Holek, *J Biol Phys*, 2009, **35**, 297–308.

53 P.-A. Monnard and D. W. Deamer, *Anat. Rec.*, 2002, **268**, 196–207.

54 K. Denzer, M. J. Kleijmeer, H. F. Heijnen, W. Stoorvogel and H. J. Geuze, *J. Cell. Sci.*, 2000, **113 Pt 19**, 3365–3374.

55 N. Yi, J. Kim, D. Jeong, M. Lee, S. C. Jang, J. Kim, Y. Gho and J. Park, Proceedings of the 16th International Conference on Miniaturized Systems for Chemistry and Life Sciences, MicroTAS 2012, 2012, pp. 1861–1863.

56 M. Colombo, G. Raposo and C. Thry, *Annu. Rev. Cell Dev. Biol.*, 2014, **30**, 255–289.

57 J. C. Stewart, *Anal. Biochem.*, 1980, **104**, 10–14.

58 A. V. Thomae, *Experimental and Theoretical Investigations on Lipid Bilayer Permeation*, Ph. D. Thesis No. 16989, Eidgenössische Technische Hochschule (ETH), Zürich, 2007.